Transmission loss of orthogonally rib-stiffened double-panel structures with cavity absorption

F. X. Xin and T. J. Lu[a)]
MOE Key Laboratory for Strength and Vibration, School of Aerospace, Xi'an Jiaotong University, Xi'an Shaanxi 710049, People's Republic of China

(Received 20 May 2010; revised 26 October 2010; accepted 4 December 2010)

The transmission loss of sound through infinite orthogonally rib-stiffened double-panel structures having cavity-filling fibrous sound absorptive materials is theoretically investigated. The propagation of sound across the fibrous material is characterized using an equivalent fluid model, and the motions of the rib-stiffeners are described by including all possible vibrations, i.e., flexural displacements, bending, and torsional rotations. The effects of fluid-structure coupling are account for by enforcing velocity continuity conditions at fluid-panel interfaces. By taking full advantage of the periodic nature of the double-panel, the space-harmonic approach and virtual work principle are applied to solve the sets of resultant governing equations, which are eventually truncated as a finite system of simultaneous algebraic equations and numerically solved insofar as the solution converges. To validate the proposed model, a comparison between the present model predictions and existing numerical and experimental results for a simplified version of the double-panel structure is carried out, with overall agreement achieved. The model is subsequently employed to explore the influence of the fluid-structure coupling between fluid in the cavity and the two panels on sound transmission across the orthogonally rib-stiffened double-panel structure. Obtained results demonstrate that this fluid-structure coupling affects significantly sound transmission loss (STL) at low frequencies and cannot be ignored when the rib-stiffeners are sparsely distributed. As a highlight of this research, an integrated optimal algorithm toward lightweight, high-stiffness and superior sound insulation capability is proposed, based on which a preliminary optimal design of the double-panel structure is performed. [DOI: 10.1121/1.3531947]

PACS number(s): 43.40.Dx, 43.55.Ti, 43.55.Rg [DF] Pages: 1919–1934

I. INTRODUCTION

Applications of lightweight, periodically rib-stiffened structures are increasingly found in mechanical, aeronautics, aerospace, and marine industries.[1–8] When these structures are applied as hulls or fuselages, external dynamic loadings (e.g., dynamic impact, sound wave impingement, and turbulent boundary layer excitation) are often encountered. The dynamic responses, sound radiation/transmission, and other relevant issues of structures have therefore been put forward and attracted much attention.

Numerous researchers have studied the sound radiation and transmission problems of periodical rib-stiffened structures.[1–5,9–13] It has been established that the rib-stiffeners play a significant role in the vibroacoustic behavior of the whole structure, especially when the bending wave length is comparable with the periodical spacing of the stiffeners.[1,5] Consequently, the equivalent forces and moments of the stiffeners should be carefully taken into account in theoretical modeling. Two different theoretical approaches have been used to address the issue.

The first one is the Fourier transform technique. Lin and Garrelick[8] employed this technique to study the transmission of sound through two infinite parallel plates connected by identical periodically spaced frames. Subsequently, a range of sound radiation problems associated with different structures, such as infinite single plates attached with identical rib-stiffeners,[1] with two different kinds of stiffeners (e.g., bulkheads and intermediate frames),[2] or with orthogonally distributed stiffeners[3] were considered using the same method, although only the equivalent forces of the stiffeners were accounted for. As an extension of Mace's work,[1] Yin *et al.*[10] theoretically analyzed the acoustic radiation from a point-driven laminated composite plate reinforced by doubly periodic parallel stiffeners, wherein the plate was modeled using the classical composite plate theory.

The other is the space-harmonic method, which is essentially equivalent to the Fourier transform technique. This approach was introduced by Mead and Pujara[4,14] to describe structural responses and acoustic pressures in terms of space-harmonic series. Based upon Mead and Pujara's works, Lee and Kim[5] developed an analytical method to study the sound transmission characteristics of a thin plate stiffened by equally spaced line stiffeners, with the resulting governing equations solved by utilizing the virtual work principle. Wang *et al.*[9] extended this approach to lightweight double-leaf partitions stiffened with periodically distributed studs, and explored the underlying sound transmission mechanisms by incorporating the dispersion relation of the structure. Following the schemes of Wang *et al.*, Legault and Atalla[11,12] analyzed the effect of structural links on sound transmission across periodically rib-stiffened double-panel structures.

[a)]Author to whom correspondence should be addressed. Electronic mail: tjlu@mail.xjtu.edu.cn

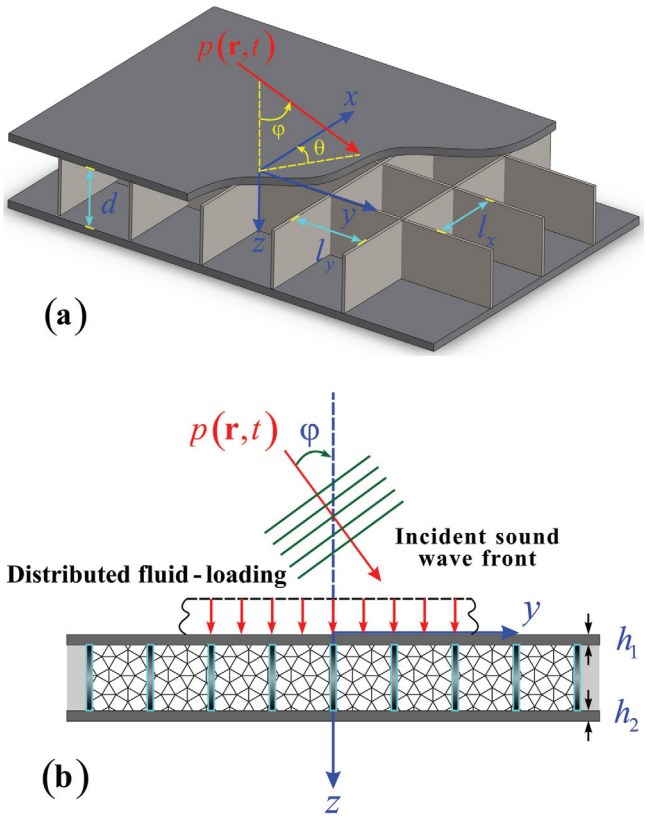

FIG. 1. (Color online) Schematic illustration of sound pressure wave incident on an orthogonally rib-stiffened double-panel structure filled with, but not necessarily limited to, fibrous sound absorptive materials: (a) global view and (b) side view of (a).

Existing studies on the vibroacoustic behavior of periodically rib-stiffened structures are often limited to one-dimensional (1D) systems. Two-dimensional (2D) orthogonally rib-stiffened double-panel structures received much less attention[3,13,15] and have not been adequately addressed, not to mention the even more complicated scenario when the cavity of the double-panel is filled with fibrous sound absorptive materials. With focus placed upon aircraft sidewalls made of rib-stiffened structures having cavity-filling fiberglass, this research proposes a relatively comprehensive theoretical model for sound transmission through orthogonally rib-stiffened double-panel structures with cavity absorption. The effect of fibrous sound absorptive filling materials on sound transmission is accounted for with an equivalent fluid model. As a highlight, an integrated optimal algorithm toward the lightweight, high-stiffness, and superior sound insulation capability is presented. A relatively rough optimal design regarding key structural geometry ratios is performed and general optimal principles are presented. The optimal scheme suggests that the integrated optimization of double-panel structures involving various physical attributes is feasible.

II. VIBROACOUSTIC RESPONSE TO CONVECTIVE HARMONIC FLUID-LOADED PRESSURE

A. Analytic formulation of panel vibration and sound transmission

With reference to Fig. 1 where (x, y, z) denote the Cartesian coordinates, consider two parallel infinite Kirchhoff thin plates lying separately in the planes of $z=0$ and $z=h_1+d$ and connected with periodically distributed rib-stiffeners along two orthogonal lines $x=ml_x$ and $y=nl_y$ (m and n both being positive or negative integer). Let d denote the thickness of the rib-stiffeners (or, cavity height), h_1 denote the thickness of the upper plate, and h_2 that of the bottom plate; see Fig. 1. The cavities in-between the two face plates and partitioned by the rib-stiffeners are filled with fibrous sound absorptive materials [see Fig. 1(b)]. The upper plate located at $z=0$ is loaded by a time-harmonic acoustic fluid $p(\mathbf{r}, t)$ with elevation angle φ and azimuth angle θ

$$p(\mathbf{r},t) = Ie^{-i(k_x x+k_y y+k_z z-\omega t)}. \quad (1)$$

The wavenumber components in the x-, y-, and z-directions are determined by the elevation angle and azimuth angle of the incident acoustic loading as

$$k_x = k_0 \sin\varphi\cos\theta,\ k_y = k_0 \sin\varphi \sin\theta,\ k_z = k_0\cos\varphi, \quad (2)$$

where $k_0=\omega/c_0$ is the acoustic wavenumber in air, ω being the angular frequency, and c_0 the sound speed in air.

As a result of the acoustic loading, a distributed load impinges on the upper plate, inducing vibration of the upper plate which is then transmitted to the bottom plate via both structure- and fluid-borne paths. The fluid-structure interaction between the bottom plate and the nearby acoustic medium causes the radiation of sound.

As shown in Fig. 1, the acoustic field is divided into three main parts by the double-panel structure: upper field occupying the half-space $z<0$, middle field filling the space $h_1<z<h_1+d$ (i.e., in-between the two face panels and partitioned periodically by the rib-stiffeners), and bottom field occupying the other half-space $z>h_1+h_2+d$. The corresponding acoustic pressure in the incident field $p_i(\mathbf{r}, t)$ should satisfy the scalar Helmholtz equation[16]

$$(\partial^2/\partial x^2 + \partial^2/\partial y^2 + \partial^2/\partial z^2)p_i + k_0^2 p_i = 0,\ z<0. \quad (3)$$

It is assumed that the cavities of the double-panel structure are filled with fibrous sound absorptive materials. As is well known, the absorption of sound by a porous absorptive material mainly arises from viscous drag forces and thermal exchange loss when sound penetrates through it.[17–20] With the help of a well-developed equivalent fluid model[21,22] for such materials, the absorbent effect induced by viscous drag force and thermal exchange between air and solid fibers is accounted for by introducing a complex wavenumber k_{cav} and a complex density ρ_{cav}. Both k_{cav} and ρ_{cav} are frequency dependent in accordance with thermal exchange transition with increasing frequency[22] (i.e., isothermal process at low frequency turning to adiabatic process at high frequency). The complex wavenumber may be expressed as $ik_{\text{cav}}=\Gamma=\alpha+i\beta$, wherein Γ is the wave propagation constant, α is the attenuation, and β is the phase constant. The corresponding acoustic pressure $p_{\text{cav}}(\mathbf{r}, t)$ in the fibrous sound absorptive material (i.e., in-between the two face plates) obeys the equation[11,23,24]

$$(\partial^2/\partial x^2 + \partial^2/\partial y^2 + \partial^2/\partial z^2)p_{\text{cav}} + k_{\text{cav}}^2 p_{\text{cav}} = 0, \quad h_1 < z < h_1 + d, \tag{4}$$

where k_{cav} is closely related to the dynamic density $p_{\text{cav}}(\omega)$ and dynamic bulk modulus $K_{\text{cav}}(\omega)$ of the fibrous sound absorptive materials as

$$k_{\text{cav}} = 2\pi f\sqrt{\rho_{\text{cav}}(\omega)/K_{\text{cav}}(\omega)}. \tag{5}$$

Applying the Johnson–Champoux–Allard model for rigid frame materials, one can obtain the dynamic density and the dynamic bulk modulus as[22,25]

$$\rho_{\text{cav}}(\omega) = \rho_0\left[1 + \frac{1}{i2\pi}\left(\frac{\sigma}{\rho_0 f}\right)G_1\left(\frac{\rho_0 f}{\sigma}\right)\right], \tag{6}$$

$$K_{\text{cav}}(\omega) = \gamma_s P_0\left(\gamma_s - \frac{\gamma_s - 1}{1 + (1/i8\pi N_{\text{pr}})(\rho_0 f/\sigma)^{-1}G_2(\rho_0 f/\sigma)}\right)^{-1}, \tag{7}$$

where $G_1(\rho_0 f/\sigma) = \sqrt{1 + i\pi(\rho_0 f/\sigma)}$, $G_2\ (\rho_0 f/\sigma) = G_1[(\rho_0 f/\sigma)\ 4N_{\text{pr}}]$, σ is the flow resistivity, γ_s is the specific heats ratio, P_0 is the air equilibrium pressure, and N_{pr} is the Prandtl number. Note that the above equivalent fluid model for filling absorbing materials is valid for f/σ smaller then 1.0 m^3/kg.[22] Generally, the flow resistivity σ of typical glass/rock wools is approximately 20 000 Nm/s^4, and hence the equivalent fluid model works well for frequencies below 20 kHz.

Finally, in the transmitted field, the acoustic pressure $p_t(\mathbf{r}, t)$ is also a solution of the scalar Helmholtz equation

$$(\partial^2/\partial x^2 + \partial^2/\partial y^2 + \partial^2/\partial z^2)p_t + k_0^2 p_t = 0, \quad z > h_1 + h_2 + d. \tag{8}$$

Assuming that the fibrous material is in perfect contact with the two plates, one can use the momentum equation to ensure the equality of plate velocity and fluid velocity at the fluid-plate interface, i.e., the continuity condition of fluid-structure coupling[8,26,27]

$$[\partial p_i/\partial z]_{z=0} = \rho_0\omega^2 w_1, \ [\partial p_{\text{cav}}/\partial z]_{z=h_1} = \rho_{\text{cav}}\omega^2 w_1, \tag{9}$$

$$[\partial p_{\text{cav}}/\partial z]_{z=h_1+d} = \rho_{\text{cav}}\omega^2 w_2, \ [\partial p_t/\partial z]_{z=h_1+h_2+d} = \rho_0\omega^2 w_2. \tag{10}$$

The complex density ρ_{cav} of the fibrous material appearing in Eqs. (9) and (10) is related to the complex wavenumber k_{cav} by[23]

$$\frac{k_{\text{cav}}^2}{k_0^2} = \frac{\gamma_s\phi\rho_{\text{cav}}}{\rho_0}, \tag{11}$$

where γ_s is the ratio of specific heats, ϕ is the porosity of the fibrous material, and ρ_0 is the air density.

The double-panel structure is driven by the difference of acoustic pressure between the two sides of each face plate. The resultant pressure imposed on the upper panel is the pressure difference between $p_t(x, y, 0; t)$ in the incident side and $p_{\text{cav}}(x, y, h_1; t)$ in the fibrous material. Similarly, the bottom panel bears the net pressure that is a subtraction of $p_{\text{cav}}(x, y, h_1 + d; t)$ in the fibrous material and $p_t(x, y, h_1 + h_2 + d; t)$ in the transmitted side. Meanwhile, with the structural constraints of the orthogonal rib-stiffeners on the face plates duly accounted for, the vibration of the plates is governed by

$$\begin{aligned} D_1\nabla^4 w_1 + m_1\frac{\partial^2 w_1}{\partial t^2} = {} & \sum_{m=-\infty}^{+\infty}\left[Q_y^+\delta(x - ml_x) + \frac{\partial}{\partial y}\left\{M_y^+\delta(x - ml_x)\right\} + \frac{\partial}{\partial x}\left\{M_{Ty}^+\delta(x - ml_x)\right\}\right] \\ & + \sum_{n=-\infty}^{+\infty}\left[Q_x^+\delta(y - nl_y) + \frac{\partial}{\partial x}\left\{M_x^+\delta(y - nl_y)\right\} + \frac{\partial}{\partial y}\left\{M_{Tx}^+\delta(y - nl_y)\right\}\right] \\ & + p_i(x, y, 0) - p_{\text{cav}}(x, y, h_1), \end{aligned} \tag{12}$$

$$\begin{aligned} D_2\nabla^4 w_2 + m_2\frac{\partial^2 w_2}{\partial t^2} = {} & -\sum_{m=-\infty}^{+\infty}\left[Q_y^-\delta(x - ml_x) + \frac{\partial}{\partial y}\left\{M_y^-\delta(x - ml_x)\right\} + \frac{\partial}{\partial x}\left\{M_{Ty}^-\delta(x - ml_x)\right\}\right] \\ & - \sum_{n=-\infty}^{+\infty}\left[Q_x^-\delta(y - nl_y) + \frac{\partial}{\partial x}\left\{M_x^-\delta(y - nl_y)\right\} + \frac{\partial}{\partial y}\left\{M_{Tx}^-\delta(y - nl_y)\right\}\right] \\ & + p_{\text{cav}}(x, y, h_1 + d) - p_i(x, y, h_1 + h_2 + d) \end{aligned} \tag{13}$$

where $\nabla^4 = (\partial^2/\partial x^2 + \partial^2/\partial y^2)^2$, $(w_1,\ w_2)$, $(m_1,\ m_2)$, and $(D_1,\ D_2)$ are the displacements, surface mass density, and bending stiffness of the upper and bottom panels, respectively, and $\delta(\cdot)$ stands for the Dirac delta function. The material loss factor $\eta_j (j = 1,2$ for upper plate and bottom plate, respectively) is introduced with the complex Young's modulus as

$$D_j = \frac{E_j h_j^3(1 + i\eta_j)}{12(1 - \nu_j^2)} \quad (j = 1, 2), \tag{14}$$

where E is the Young's modulus and ν the Poisson ratio of the plate material.

Due to the consideration of inertial effects, the resultant transverse forces, bending moments, and torsional moments exerted on the upper and bottom plates are not identical, denoted here separately as (Q^+, M^+, M_T^+) and (Q^-, M^-, M_T^-). Superscripts + and − denote separately the upper and bottom plates, while subscripts x and y signify the terms arising from the x- and y-wise rib-stiffeners, respectively. An illustration of the present conventions for transverse forces, bending moments and torsional moments is given in Fig. 2. Detailed derivations of these quantities can be found in Appendix A.

B. Application of the periodicity of structures

Taking advantage of the periodical property of the orthogonally rib-stiffened double-panel structures considered here, one can simplify the theoretical formulations presented

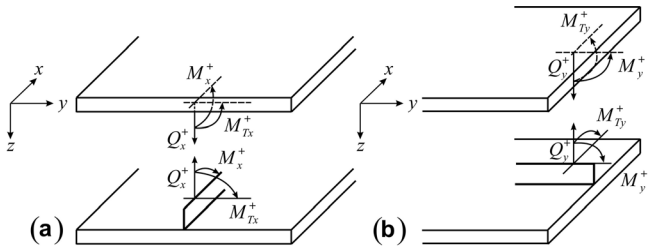

FIG. 2. Conventions for tensional forces, bending moments, and torsional moments at the interface between upper plate and (a) x-wise stiffeners and (b) y-wise stiffeners. The same apply at the interface between bottom plate and x/y-wise stiffeners.

above to obtain analytical solutions of the problem. As mentioned in an earlier work,[13] following the key conclusion of Bloch or Floquet's theorem[28] for wave propagation in periodic structures, the displacements $w(x, y)$ of such a system at the corresponding points in different periodic elements are related by the periodicity condition as

$$w(x+ml_x, y+nl_y) = w(x,y)e^{-ik_x ml_x}e^{-ik_y ml_y}, \times (m,n \text{ being integers}). \quad (15)$$

The space-harmonic expansion series can thence be favorably applied to express the panel displacement $w_j(x, y; t)$ as [3,4,13,29]

$$w_j(x,y;t) = \sum_{m=-\infty}^{+\infty}\sum_{n=-\infty}^{+\infty} \alpha_{1,mn} e^{-i[(k_x+2m\pi/l_x)x+(k_y+2n\pi/l_y)y-\omega t]} \times (j=1,2) \quad (16)$$

where $j=1$ for the upper panel, $j=2$ for the bottom panel, the (m, n)th harmonic wave has wavenumber components $(k_x+2m\pi/l_x, k_y+2n\pi/l_y)$, illustrating its propagation direction in the structure and

$$\alpha_{j,mn} = \frac{1}{l_x l_y}\int_0^{l_x}\int_0^{l_y} w_1(x,y;t)e^{i[(k_x+2m\pi/l_x)x+(k_y+2n\pi/l_y)y-\omega t]} \times dxdy (j=1,2). \quad (17)$$

Due to sound pressure $p(\mathbf{r}, t) = Ie^{-i(\mathbf{k}\cdot\mathbf{r}-\omega t)}$ incident on the double-panel, the set of sound pressures can be expressed as[13,29]

$$p_j(x,y,z;t) = Ie^{-i(k_x x+k_y y+k_z z-\omega t)} + \sum_{m=-\infty}^{+\infty}\sum_{n=-\infty}^{+\infty} \times \beta_{mn} e^{-i[(k_x+2m\pi/l_x)x+(k_y+2n\pi/l_y)y-k_{z,mn}z-\omega t]}, \quad (18)$$

$$p_{\text{cav}}(x,y,z;t) = \sum_{m=-\infty}^{+\infty}\sum_{n=-\infty}^{+\infty} \varepsilon_{mn} e^{-i[(k_x+2m\pi/l_x)x+(k_y+2n\pi/l_y)y-k_{z,\text{cav},mn}z-\omega t]} + \sum_{m=-\infty}^{+\infty}\sum_{n=-\infty}^{+\infty} \zeta_{mn} e^{-i[(k_x+2m\pi/l_x)x+(k_y+2n\pi/l_y)y-k_{z,\text{cav},mn}z-\omega t]}, \quad (19)$$

$$p_t(x,y,z;t) = \sum_{m=-\infty}^{+\infty}\sum_{n=-\infty}^{+\infty} \xi_{mn} e^{-i[(k_x+2m\pi/l_x)x+(k_y+2n\pi/l_y)y-k_{z,mn}z-\omega t]}. \quad (20)$$

In the above expressions, I is the amplitude of incident sound pressure, β_{mn} and ζ_{mn} are the (m, n)th space-harmonic amplitude of negative-going wave in the incident field and in the middle field, respectively, and ε_{mn} and ξ_{mn} are the (m, n)th space-harmonic amplitude of positive-going wave in the middle filed and in the transmitted field, respectively. Furthermore, $k_{z,mn}$ and $k_{z,\text{cav},mn}$ are the (m, n)th space-harmonic wavenumbers in the z-direction (related separately to wave propagation in air and fibrous absorptive material) which, upon applying the Helmholtz equation, are given by[9,11,12]

$$k_{z,mn} = \sqrt{k_0^2-\alpha_m^2-\beta_n^2},\ k_{z,\text{cav},mn} = \sqrt{k_{\text{cav}}^2-\alpha_m^2-\beta_n^2} \quad (21)$$

where the (m, n)th harmonic wavenumber components in the x- and y-directions are expressed as

$$\alpha_m = k_x + 2m\pi/l_x,\ \beta_n = k_y + 2n\pi/l_y. \quad (22)$$

Given that the z-direction wavenumber component is determined by Eq. (21), two different modes of sound propagation in the transmitting field can be distinguished:[13,30] (i) non-radiating wave (i.e., subsonic wave) when $\alpha_m^2+\beta_n^2 > k_0^2$ and (ii) radiating wave (i.e., supersonic wave) when $\alpha_m^2+\beta_n^2 < k_0^2$. Whilst the (m, n)th sound wave component contributes only to the near field in the first case, it is able to contribute to the far field in the second case.

Substitution of Eqs. (16) and (18)–(20) into Eqs. (9) and (10) yields

$$-ik_z Ie^{-i(k_x x+k_y y)} + \sum_{m=-\infty}^{+\infty}\sum_{n=-\infty}^{+\infty}\left(ik_{mn}\beta_{mn} - \rho_0\omega^2\alpha_{1,mn}\right) \times e^{-i(\alpha_m x+\beta_n y)} = 0, \quad (23)$$

$$\sum_{m=-\infty}^{+\infty}\sum_{n=-\infty}^{+\infty}\begin{bmatrix} ik_{z,\text{cav},mn}\left(-\varepsilon_{mn}e^{-ik_{z,\text{cav},mn}h_1} + \zeta_{mn}e^{ik_{z,\text{cav},mn}h_1}\right) \\ -\rho_{\text{cav}}\omega^2\alpha_{1,mn}\end{bmatrix} \times e^{-i(\alpha_m x+\beta_n y)} = 0, \quad (24)$$

$$\sum_{m=-\infty}^{+\infty}\sum_{n=-\infty}^{+\infty}\begin{bmatrix} ik_{z,\text{cav},mn}\left(-\varepsilon_{mn}e^{-ik_{z,\text{cav},mn}(h_1+d)} + \zeta_{mn}e^{ik_{z,\text{cav},mn}(h_1+d)}\right) \\ -\rho_{\text{cav}}\omega^2\alpha_{2,mn}\end{bmatrix} \times e^{-i(\alpha_m x+\beta_n y)} = 0, \quad (25)$$

$$\sum_{m=-\infty}^{+\infty}\sum_{n=-\infty}^{+\infty}\left[-ik_{z,mn}\xi_{mn}e^{-ik_{z,mn}(h_1+h_2+d)} - \rho_0\omega^2\alpha_{2,mn}\right] \times e^{-i(\alpha_m x+\beta_n y)} = 0. \quad (26)$$

Because Eqs. (23)–(26) hold for all possible values of x and y, it can be shown that the relevant coefficients have the following relationships:

$$\beta_{00} = I + \frac{\omega^2\rho_0\alpha_{1,00}}{ik_z}, \quad (27)$$

$$\beta_{mn} = \frac{\omega^2\rho_0\alpha_{1,mn}}{ik_{z,mn}}, \text{ at } m\neq 0 || n\neq 0, \quad (28)$$

$$\varepsilon_{mn} = \frac{\omega^2 \rho_{\text{cav}} \left[\alpha_{1,mn} e^{ik_{z,\text{cav},mn}(h_1+d)} - \alpha_{2,mn} e^{ik_{z,\text{cav},mn}h_1}\right]}{2k_{z,\text{cav},mn} \sin(k_{z,\text{cav},mn} d)}, \quad (29)$$

$$\zeta_{mn} = \frac{\omega^2 \rho_{\text{cav}} \left[\alpha_{1,mn} e^{-ik_{z,\text{cav},mn}(h_1+d)} - \alpha_{2,mn} e^{-ik_{z,\text{cav},mn}h_1}\right]}{2k_{z,\text{cav},mn} \sin(k_{z,\text{cav},mn} d)}, \quad (30)$$

$$\xi_{mn} = -\frac{\omega^2 \rho_0 \alpha_{2,mn}}{ik_{z,mn}} e^{ik_{z,mn}(h_1+h_2+d)}. \quad (31)$$

Here, it is worth mentioning that the framing structures are taken to be acoustically transparent, i.e., they do not block acoustic wave in the cavity. In future studies, it will be important to explore this aspect of the problem.

C. Solution by employing the virtual work principle

Since the double-panel structure considered here is spatially periodic, the principle of virtual work[4,5,9] can be utilized to solve the theoretical formulations presented above and thence obtain the values of coefficients $\alpha_{1,mn}$ and $\alpha_{2,mn}$. As close relationships exist between the coefficients of panel displacements (i.e., $\alpha_{1,mn}$ and $\alpha_{2,mn}$) and those of sound pressure (i.e., β_{mn}, ε_{mn}, ζ_{mn}, and ξ_{mn}), the sound pressures can be straightforwardly obtained once the former is determined. To calculate the virtual work done by imposing the virtual displacements,

$$\delta w_j^* = \delta\alpha_{j,kl} e^{-i(a_k x+\beta_l y)} \ (j=1,2), \quad (32)$$

on the double-panel, only one periodical element needs to be considered. The principle of virtual work states that the virtual work of the system stemming from the virtual displacements should be zero, from which the equilibrium equation of system can be established as detailed below.

1. Virtual work of panel elements

The virtual work contributed solely by one periodical element of each plate can be represented as

$$\delta\Pi_{p1} = \int_0^{l_x}\int_0^{l_y} \left[D_1\nabla^4 w_1 + m_1\frac{\partial^2 w_1}{\partial t^2} - p_i(x,y,0) + p_{\text{cav}}(x,y,h_1)\right] \times \delta w_1 dxdy = \left\{\left[D_1(\alpha_k^2+\beta_l^2) - m_1\omega^2\right]\alpha_{1,kl} - \frac{\omega^2\rho_0\alpha_{1,kl}}{ik_{z,kl}} + \frac{\omega^2 p_{\text{cav}}\alpha_{1,kl}\cos(k_{z,\text{cav},kl}d) - \alpha_{2,kl}]}{k_{z,\text{cav},kl}\sin(k_{z,\text{cav},kl}d)}\right\} \cdot l_x l_y \delta\alpha_{1,kl} - \int_0^{l_x}\int_0^{l_y} 2le^{-i(k_x x+k_y y)} e^{i(a_k x+\beta_l y)} dxdy \cdot \delta\alpha_{1,kl}, \quad (33)$$

$$\delta\Pi_{p2} = \int_0^{l_x}\int_0^{l_y} \left[D_2\nabla^4 w_2 + m_2\frac{\partial^2 w_2}{\partial t^2} - p_{\text{cav}}(x,y,h_1+d) + p_i(x,y,h_1+h_2+d)\right] \cdot \delta w_2 dxdy = \left\{\left[D_2(\alpha_k^2+\beta_l^2) - m_2\omega^2\right]\alpha_{2,kl} - \frac{\omega^2\rho_0\alpha_{2,kl}}{ik_{z,kl}} - \frac{\omega^2 p_{\text{cav}}\left[\alpha_{1,kl} - \alpha_{2,kl}\cos(k_{z,\text{cav},kl}d)\right]}{k_{z,\text{cav},kl}\sin(k_{z,\text{cav},kl}d)}\right\} \cdot l_x l_y \delta\alpha_{2,kl}, \quad (34)$$

2. Virtual work of x-wise stiffeners

The virtual work contribution from the transverse force, bending moment and torsional moment at the interface between the x-wise stiffeners (aligned with $y=0$) and upper or bottom panel is given by[13]

$$\delta\Pi_{x1} = -\int_0^{l_x}\left[Q_x^+(x,0) + \frac{\partial}{\partial x}M_x^+(x,0) + \frac{\partial}{\partial y}M_{Tx}^+(x,0)\right] \times \delta\alpha_{1,kl} e^{ia_k x} dx = \sum_{n=-\infty}^{+\infty} [R_{Q1}\alpha_{1,kn} - R_{Q2}\alpha_{2,kn} + i\alpha_k^3(-R_{M1}\alpha_{1,kn} + R_{M2}\alpha_{2,kn}) + i\alpha_k\beta_l\beta_n(-R_{T1}\alpha_{1,kn} + R_{T2}\alpha_{2,kn})] l_x \delta\alpha_{1,kl}, \quad (35)$$

$$\delta\Pi_{x2} = \int_0^{l_x}\left[Q_x^-(x,0) + \frac{\partial}{\partial x}M_x^-(x,0) + \frac{\partial}{\partial y}M_{Tx}^-(x,0)\right] \cdot \delta\alpha_{2,kl} e^{ia_k x} dx = \sum_{n=-\infty}^{+\infty} [-R_{Q2}\alpha_{1,kn} + R_{Q1}\alpha_{2,kn} - i\alpha_k^3(-R_{M2}\alpha_{1,kn} + R_{M1}\alpha_{2,kn}) - i\alpha_k\beta_l\beta_n(-R_{T2}\alpha_{1,kn} + R_{T1}\alpha_{2,kn})] l_x \delta\alpha_{2,kl}, \quad (36)$$

where $\frac{\partial M_{Tx}^+(x,0)}{\partial y} = \frac{\partial M_{Tx}^+(x,y)}{\partial y}\Big|_{y=o}$ and $\frac{\partial M_{Tx}^-(x,0)}{\partial y} = \frac{\partial M_{Tx}^-(x,y)}{\partial y}\Big|_{y=o}$.

3. Virtual work of y-wise stiffeners

Likewise, the virtual work done by the transverse force, bending moment, and torsional moment at the interface between the y-wise stiffeners (aligned with $x=0$) and upper or bottom panel is[13]

$$\delta\Pi_{y1} = -\int_0^{l_y}\left[Q_y^+(0,y) + \frac{\partial}{\partial y}M_y^+(0,y) + \frac{\partial}{\partial x}M_{Ty}^+(0,y)\right] \cdot \delta\alpha_{1,kl} e^{i\beta_l y} dy = \sum_{m=-\infty}^{+\infty}\left[\begin{matrix} R_{Q3}\alpha_{1,ml} - R_{Q4}\alpha_{2,ml} + i\beta_l^3(-R_{M3}\alpha_{1,ml} + R_{M4}\alpha_{2,ml}) \\ +i\alpha_k\alpha_m\beta_l(-R_{T3}\alpha_{1,ml} + R_{T4}\alpha_{2,ml}) \end{matrix}\right] \cdot l_y \delta\alpha_{1,kl}, \quad (37)$$

$$\delta\Pi_{y2} = \int_0^{l_y} \left[Q_y^-(0,y) + \frac{\partial}{\partial y} M_y^-(0,y) + \frac{\partial}{\partial x} M_{Ty}^-(0,y) \right] \cdot \delta\alpha_{2,kl} e^{i\beta_l y} dy$$

$$= \sum_{m=-\infty}^{+\infty} \begin{bmatrix} -R_{Q4}\alpha_{1,ml} + R_{Q3}\alpha_{2,ml} - i\beta_l^3(-R_{M4}\alpha_{1,ml} + R_{M3}\alpha_{2,ml}) \\ -i\alpha_k\alpha_m\beta_l(-R_{T4}\alpha_{1,ml} + R_{T3}\alpha_{2,ml}) \end{bmatrix} \cdot l_y \delta\alpha_{2,kl}, \tag{38}$$

where $\frac{\partial M_{Ty}^+(0,y)}{\partial x} = \frac{\partial M_{Ty}^+(x,y)}{\partial x}\Big|_{x=o}$ and $\frac{\partial M_{Ty}^-(0,y)}{\partial x} = \frac{\partial M_{Ty}^-(x,y)}{\partial x}\Big|_{x=o}$.

4. Resultant equations for structure motions

It follows from the virtual work principle that

$$\delta\Pi_{p1} + \delta\Pi_{x1} + \delta\Pi_{y1} = 0,\ \delta\Pi_{p2} + \delta\Pi_{x2} + \delta\Pi_{y2} = 0. \tag{39}$$

Substituting Eqs. (33)–(38) into Eq. (39) and noticing that the virtual displacement is arbitrary, one obtains

$$\begin{aligned}
&\left\{ \left[D_1(\alpha_k^2 + \beta_l^2)^2 - m_1\omega^2 \right] \alpha_{1,kl} - \frac{\omega^2\rho_0\alpha_{1,kl}}{ik_{z,kl}} \right. \\
&\left. + \frac{\omega^2\rho_{\text{cav}}\left[\alpha_{1,kl}\cos(k_{z,\text{cav},kl}d) - \alpha_{2,kl}\right]}{k_{z,\text{cav},kl}\sin(k_{z,\text{cav},kl}d)} \right\} \cdot l_x l_y \\
&+ \sum_{n=-\infty}^{+\infty} \left[R_{Q1}\alpha_{1,kn} - R_{Q2}\alpha_{2,kn} + i\alpha_k^3(R_{M2}\alpha_{2,kn} - R_{M1}\alpha_{1,kn}) \right. \\
&\left. + i\alpha_k\beta_n\beta_l(R_{T2}\alpha_{2,kn} - R_{T1}\alpha_{1,kn}) \right] \cdot l_x \\
&+ \sum_{m=-\infty}^{+\infty} \left[R_{Q3}\alpha_{1,ml} - R_{Q4}\alpha_{2,ml} + i\beta_l^3(R_{M4}\alpha_{2,ml} - R_{M3}\alpha_{1,ml}) \right. \\
&\left. + i\alpha_m\alpha_k\beta_l(R_{T4}\alpha_{2,ml} - R_{T3}\alpha_{1,ml}) \right] \cdot l_y \\
&= \begin{cases} 2Il_x l_y & \text{when } k = 0 \text{ and } l = 0 \\ 0 & \text{when } k \neq 0 || l \neq 0 \end{cases},
\end{aligned} \tag{40}$$

$$\begin{aligned}
&\left\{ \left[D_2(\alpha_k^2 + \beta_l^2)^2 - m_2\omega^2 \right] \alpha_{2,kl} - \frac{\omega^2\rho_0\alpha_{2,kl}}{ik_{z,kl}} \right. \\
&\left. - \frac{\omega^2\rho_{\text{cav}}\left[\alpha_{1,kl} - \alpha_{2,kl}\cos(k_{z,\text{cav},kl}d)\right]}{k_{z,\text{cav},kl}\sin(k_{z,\text{cav},kl}d)} \right\} \cdot l_x l_y \\
&+ \sum_{n=-\infty}^{+\infty} \left[-R_{Q2}\alpha_{1,kn} + R_{Q1}\alpha_{2,kn} - i\alpha_k^3(R_{M1}\alpha_{2,kn} - R_{M2}\alpha_{1,kn}) \right. \\
&\left. - i\alpha_k\beta_n\beta_l(R_{T1}\alpha_{2,kn} - R_{T2}\alpha_{1,kn}) \right] \cdot l_x \\
&+ \sum_{m=-\infty}^{+\infty} \left[-R_{Q4}\alpha_{1,ml} + R_{Q3}\alpha_{2,ml} \right. \\
&- i\beta_l^3(R_{M3}\alpha_{2,ml} - R_{M4}\alpha_{1,ml}) \\
&\left. - i\alpha_m\alpha_k\beta_l(R_{T3}\alpha_{2,ml} - R_{T4}\alpha_{1,ml}) \right] \cdot l_y = 0.
\end{aligned} \tag{41}$$

It should be mentioned that the consideration of virtual work in any other periodical element of the double-panel structure would have yielded an identical set of equations.

In order to separate the variables $\alpha_{1,kl}$ and $\alpha_{2,kl}$, Eqs. (40) and (41) are rewritten as:

$$\begin{aligned}
&\left[D_1(\alpha_k^2 + \beta_l^2)^2 - m_1\omega^2 - \frac{\omega^2\rho_0}{ik_{z,kl}} + \frac{\omega^2\rho_{\text{cav}}\cos(k_{z,\text{cav},kl}d)}{k_{z,\text{cav},kl}\sin(k_{z,\text{cav},kl}d)} \right] \\
&\times l_x l_y \alpha_{1,kl} - \frac{\omega^2\rho_{\text{cav}}}{k_{z,\text{cav},kl}\sin(k_{z,\text{cav},kl}d)} \cdot l_x l_y \alpha_{2,kl} \\
&+ \sum_{n=-\infty}^{+\infty} \left[R_{Q1} - i\alpha_k^3 R_{M1} - i\beta_l\alpha_k\beta_n R_{T1} \right] \cdot l_x \alpha_{1,kn} \\
&+ \sum_{n=-\infty}^{+\infty} \left[-R_{Q2} + i\alpha_k^3 R_{M2} + i\beta_l\alpha_k\beta_n R_{T2} \right] \cdot l_x \alpha_{2,kn} \\
&+ \sum_{m=-\infty}^{+\infty} \left[R_{Q3} - i\beta_l^3 R_{M3} - i\alpha_k\alpha_m\beta_l R_{T3} \right] \cdot l_y \alpha_{1,ml} \\
&+ \sum_{m=-\infty}^{+\infty} \left[-R_{Q4} + i\beta_l^3 R_{M4} + i\alpha_k\alpha_m\beta_l R_{T4} \right] \cdot l_y \alpha_{2,ml} \\
&= \begin{cases} 2Il_x l_y & \text{when } k = 0 \text{ and } l = 0 \\ 0 & \text{when } k \neq 0 || l \neq 0 \end{cases},
\end{aligned} \tag{42}$$

$$\begin{aligned}
&\left[D_2(\alpha_k^2 + \beta_l^2)^2 - m_2\omega^2 - \frac{\omega^2\rho_0}{ik_{z,kl}} + \frac{\omega^2\rho_{\text{cav}}\cos(k_{z,\text{cav},kl}d)}{k_{z,\text{cav},kl}\sin(k_{z,\text{cav},kl}d)} \right] \\
&\times l_x l_y \alpha_{2,kl} - \frac{\omega^2\rho_{\text{cav}}}{k_{z,\text{cav},kl}\sin(k_{z,\text{cav},kl}d)} \cdot l_x l_y \alpha_{1,kl} \\
&+ \sum_{n=-\infty}^{+\infty} \left[-R_{Q2} + i\alpha_k^3 R_{M2} + i\beta_l\alpha_k\beta_n R_{T2} \right] \cdot l_x \alpha_{1,kn} \\
&+ \sum_{n=-\infty}^{+\infty} \left[R_{Q1} - i\alpha_k^3 R_{M1} - i\beta_l\alpha_k\beta_n R_{T1} \right] \cdot l_x \alpha_{2,kn} \\
&+ \sum_{m=-\infty}^{+\infty} \left[-R_{Q4} + i\beta_l^3 R_{M4} + i\alpha_k\alpha_m\beta_l R_{T4} \right] \cdot l_y \alpha_{1,ml} \\
&+ \sum_{m=-\infty}^{+\infty} \left[R_{Q3} - i\beta_l^3 R_{M3} - i\alpha_k\alpha_m\beta_l R_{T3} \right] \cdot l_y \alpha_{2,ml} = 0.
\end{aligned} \tag{43}$$

The infinite set of coupled algebraic simultaneous equation system of Eqs. (42) and (43) can be simplified as a finite set of equations by applying a truncated series of the assumed modes, insofar as the solution converges. In the present study, the sum-indices (m, n) are restricted to have finite values, i.e., $m = -\hat{k}$ to $\hat{k}$ and $n = -\hat{l}$ to $\hat{l}$. Upon necessary algebraic manipulations (Appendix B), the resultant equation system that contains a finite number (i.e., $2KL$, where $K = 2\hat{k} + 1$, $L = 2\hat{l} + 1$) of unknowns can be expressed in matrix notation as

$$\begin{bmatrix} T_{11,kl} & T_{12,kl} \\ T_{21,kl} & T_{22,kl} \end{bmatrix}_{2KL\times 2KL} \begin{Bmatrix} \alpha_{1,kl} \\ \alpha_{2,kl} \end{Bmatrix}_{2KL\times 1} = \begin{Bmatrix} F_{kl} \\ 0 \end{Bmatrix}_{2KL\times 1}. \tag{44}$$

Solving Eq. (44) one can obtain the vibration displacements of the two face plates, with which the acoustic pressures in different fields are readily determined. As an assessment of sound energy penetrating through the structure, the transmission coefficient is defined here as the ratio of the transmitted sound power to the incident sound power as[9,11,13]

$$\tau(\varphi,\theta)=\frac{\sum_{m=-\infty}^{+\infty}\sum_{n=-\infty}^{+\infty}|\xi_{mn}|^2\mathrm{Re}\left(k_{z,mn}\right)}{|I|^2k_z}, \tag{45}$$

which is a function of sound incident angles φ and θ. The diffuse sound transmission coefficient is taken in an averaged form over all possible incident angles[29] as

$$\tau_{diff}=\frac{\int_0^{\pi/4}\int_0^{\varphi_{\lim}}\tau(\varphi,\theta)\sin\varphi\cos\varphi d\varphi d\theta}{\int_0^{\pi/4}\int_0^{\varphi_{\lim}}\sin\varphi\cos\varphi d\varphi d\theta}. \tag{46}$$

Finally, sound transmission loss (STL) is customarily defined in decibel scale[6,7] as

$$STL=10\log_{10}\left(\frac{1}{\tau(\varphi,\theta)}\right), \tag{47}$$

which, intuitively, may be taken as a measure of the effectiveness of the double-panel structure in insulating the sound energy penetration.

III. PARAMETRIC INVESTIGATION AND DISCUSSION

In this section, the theoretical model developed above is used to examine the vibroacoustic performance of the type of double-panel structures shown in Fig. 1 and explore the physical mechanisms underlying the sound transmission process.

In subsequent numerical calculations, unless otherwise specified, the following sets of system parameters are adopted: the two face plates are identical, each having thickness $h_1=h_2=0.002$ m; the orthogonal rib-stiffeners have depth $d=0.08$ m, thickness $t_x=t_y=0.001$ m, and periodicity spacing $l_x=l_y=0.2$ m (Fig. 1). The face plates and the rib-stiffeners are made of the same material, with Young's modulus $E=70$ GPa, density $\rho=2700$ kg/m^3, Poisson ratio $v=0.33$, and loss factor $\eta=0.01$. In the common situation of normal temperature and atmospheric pressure, it can be assumed that $\rho_0=1.21$ kg/m^3, $N_{\mathrm{pr}}=0.702$, $\gamma_s=1.4$, $P_0=10\,1320$ N/m^2, and $c_0=343$ m/s. The widely applied fiberglass is selected as the cavity-filling fibrous material, with porosity $\phi=0.95$ and flow resistivity $\sigma=24\,000$ Nm/s^4.

Since the numerical results are calculated based on the assumed space-harmonic series solution, a sufficiently large number of terms should be applied to ensure the convergence and accuracy of the solution. Following the convergence check scheme that has been proposed in our previous publication,[13] a convergence check study for the present absorptive material filling case is performed. It has been obtained that the space-harmonic series solution needs at least 1849 terms (m and n both ranging from -21 to 21) to ensure the solution convergence at 10 kHz. The same number (1849 terms) is then adopted to calculate all STL values below 10 kHz, which is sufficient to achieve accurate results within the error bound of 0.01 dB.

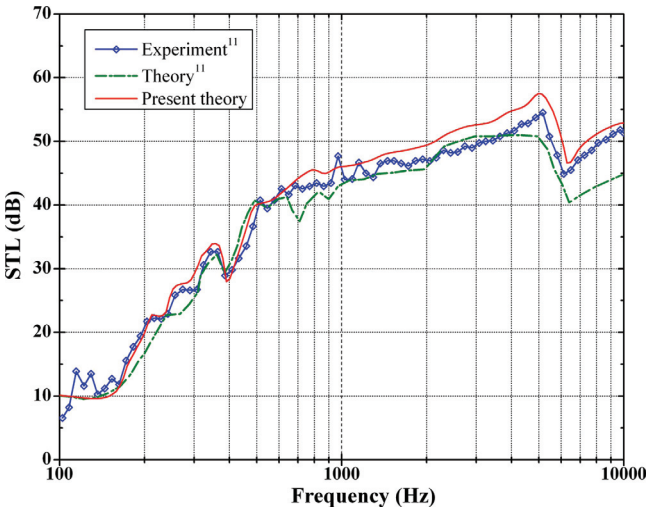

FIG. 3. (Color online) Diffuse (STL) plotted as a function of incident frequency: comparison between present model predictions with experimental measurements and theoretical results of Legault and Atalla.[11]

A. Model validation

For validation, the present model predictions are compared with the theoretical results and experimental measurements of Legault and Atalla[11] for 1D periodically rib-stiffened double-panel structures, as shown in Fig. 3. Since our model is developed for *orthogonally* rib-stiffened double-panel structures, it can be favorably degraded to the 1D case.

As can be seen in Fig. 3, an overall agreement is achieved. Especially, the experimentally observed two significant resonance dips have been well captured by the present model, i.e., the first dip at approximately 400 Hz arising from the pass band characteristics of periodic structures, and the other due to coincidence resonance[11] at the critical frequency of approximately 6200 Hz.

Since the diffuse sound transmission characteristics of periodically rib-stiffened double-panel structure have been well studied by Legault and Atalla,[11] the focus of the present study thus turns to the normal sound incident case so as to explore more physical details. Moreover, in view of the fact that the sound transmission behavior of three different double-panel structures as considered below is quite similar with dense peaks and dips at high frequencies, the frequency range of 10–2000Hz is considered in all subsequent analyses. As a result, the coincidence resonance dip is far beyond the considered frequency range which, even if calculated, would merge with the dense dips at high frequencies and impossible to distinguish in single incidence STL results. However, as shown in Fig. 3, the coincidence resonance dip can be clearly identified in diffuse STL results after weighted average operation [see Eq. (46)].

B. Effects of fluid-structure coupling on sound transmission

Since the absorption of sound by fibrous materials (i.e., fiberglass) is characterized using the frequency-dependent

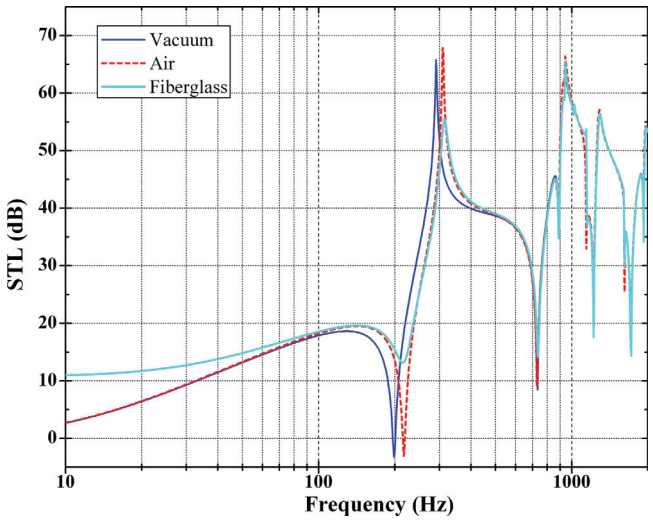

FIG. 4. (Color online) STL plotted as a function of incident frequency for stiffener separations $l_x = l_y = 0.3$ m: comparison amongst three different kinds of orthogonally rib-stiffened double-panels with cavities filled separately with vacuum, air, and fiberglass.

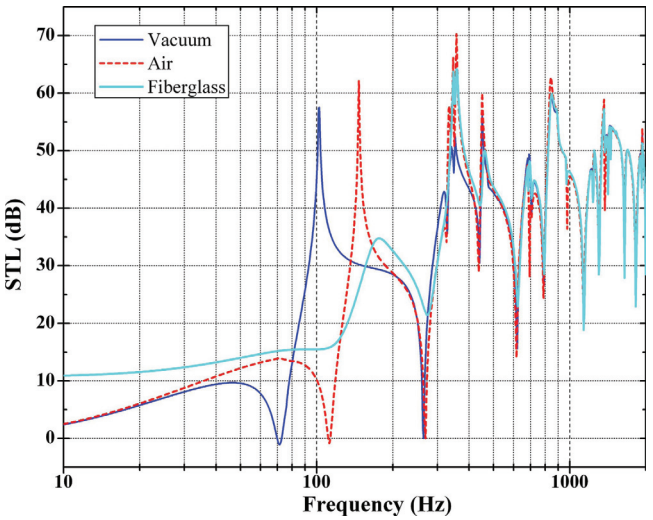

FIG. 6. (Color online) STL plotted as a function of incident frequency for stiffener separations $l_x = l_y = 0.5$ m: comparison amongst three different kinds of orthogonally rib-stiffened double-panels with cavities filled separately with vacuum, air, and fiberglass.

dynamic density and bulk modulus, the fluid-structure coupling effects (between fluid in the cavity and the two panels) are exploited below. For comparison, the air cavity case and the vacuum case are also considered to highlight the influence of the cavity-filling fiberglass.

Figures 4–6 plot the STL as a function of frequency for the three different cases, with the periodic spacings selected as $l_x = l_y = 0.3$, 0.4, and 0.5 m, respectively. The results of Figs. 4–6 demonstrate that fluid-structure coupling can alter the STL peaks and dips in the low frequency range and thus affect sound transmission, especially when the rib-stiffeners are sparsely distributed (e.g., $l_x = l = 0.5$ m). In such cases, the response of the face panels is significantly affected by the fluid media confined in the cavities, since most of the panel surfaces are in contact with the fluid and the rib-stiffeners may only exert a local effect near the conjunctions. In other words, when the rib-stiffener separation is sufficiently large, fluid-structure coupling plays a role comparable to that of the rib-stiffeners. Under such conditions, the fluid-structure coupling effect can no longer be assumed negligible particularly in the stiffness-controlled low frequency range.

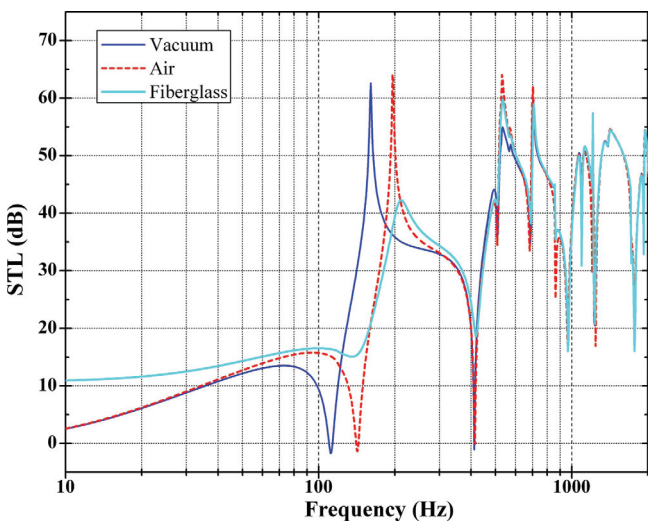

FIG. 5. (Color online) STL plotted as a function of incident frequency for stiffener separations $l_x = l_y = 0.4$ m: comparison amongst three different kinds of orthogonally rib-stiffened double-panels with cavities filled separately with vacuum, air, and fiberglass.

As can be observed from the results of Figs. 4–6, the three cases considered differ mainly in the low frequency range where the fluid media confined in the partitioned cavities act on the face panels through fluid-structure coupling effect and work like pumping. That is, similar to elastic springs, the fluid media have equivalent stiffness, which affects significantly sound transmission in the stiffness-controlled low frequency range whilst has almost no influence in the mass-controlled high frequency range. As the stiffener separation is increased, the equivalent stiffness of the fluid media plays an increasingly important role in the transmission of sound, as the surface area of the face panels dominated by fluid media increases whilst that controlled by the rib-stiffeners decreases. With this duly considered, it is then understandable that the divergences only exist in the low frequency range, enlarging with increasing stiffener separation, as demonstrated in Figs. 4–6.

As interpreted in our previous publication,[9] the dips appearing in the STL curves in Figs. 4–6 correspond to frequencies at which the incident sound wave undergoes a kind of resonance with the free wave propagation of vibration in the panels. The effect is analogous to the familiar "coincidence frequency," but the spatial harmonics created by wave reflection at the rib-stiffeners introduce multiple possibilities for wavenumber matching and "coincidence." These dips in STL curves can be clearly explained by the dispersion relation of the periodic structure, that is, the "pass band" and "stop band" characteristics of wave propagation. For more details one may refer to the interpretations given for Figs. 9 (a)–9(c) in our previous publication.[9] In addition, similar explanations that the dips arise from the pass band characteristics of periodic structures are also proposed by Legault and Atalla.[11]

Furthermore, relative to the vacuum case, it is seen that the first dips in Figs. 4–6 all shift to higher frequencies in the air cavity as well as fiberglass filling cases. This is because either air or fiberglass can work like springs and thus increase the stiffness of the structure. As shown in Figs. 4–6, the attenuation added by the fluid (i.e., fiberglass equivalent fluid) is clearly exhibited by the smoother dips in the fiberglass filling case compared to the two other cases. Taking an overall view of Figs. 4–6, one can observe that the dips shift to lower frequencies when the stiffener separation is increased. This is because the increment of stiffener separation changes the periodicity of the structure, resulting in the alteration of its dispersion relation, eventually causing the decrease of its natural frequencies.

C. STL combined with bending stiffness and structure mass: Optimal design of double-panel

Due to high-stiffness-to-weight ratio, double-panel structures have been widely applied in aeronautics and aerospace engineering, often providing acceptable sound insulation capability. To draw general guidelines for the practical engineering design of these weight-sensitive structures, an optimal design scheme for multi-functional double-panels is presented and implemented below, combining low structure mass with high-stiffness and superior sound insulation requirements.

Since both the face panels and rib-stiffeners considered in the present study have thin thickness compared with other geometrical dimensions, such as core depth d and periodical spacing l_x (or l_y), the most important structural geometry ratio only leaves the non-dimensional variable l_x/d (or l_y/d). For simplicity, assuming that $l_x = l_y$, then it only needs to consider one variable (l/d) to seek for the optimal design of the double-panel for combined high STL, large bending stiffness and low structure mass. Although diffuse STL may be of more interest for practical engineering, the normal sound incident case is considered here to save computational efforts. To this end, several dimensionless parameters should be defined.

The first dimensionless parameter introduced is the normalized mass of the double-panel (i.e., ratio of the mass for one unit cell to that of the panel material filling the whole volume of the unit cell)

$$\bar{M} = \frac{\rho\left[(h_1+h_2)l_x l_y + (l_x t_x + l_y t_y)d\right] + \rho_{\text{cav}} l_x l_y d}{\rho l_x l_y (d+h_1+h_2)}. \quad (48)$$

The above expression has accounted for the cavity-filling fiberglass. For the air cavity case, one only needs to eliminate the fiberglass term.

For external load bearing, the bending stiffness of the orthogonally rib-stiffened double-panel structure is important, given by[31,32]

$$D_x = \frac{2Eh^3}{12} + \frac{Eh(d+h)^2}{2} + \frac{Ed^3}{12}\frac{t_x}{l_y},$$
$$D_y = \frac{2Eh^3}{12} + \frac{Eh(d+h)^2}{2} + \frac{Ed^3}{12}\frac{t_y}{l_x}, \quad (49)$$

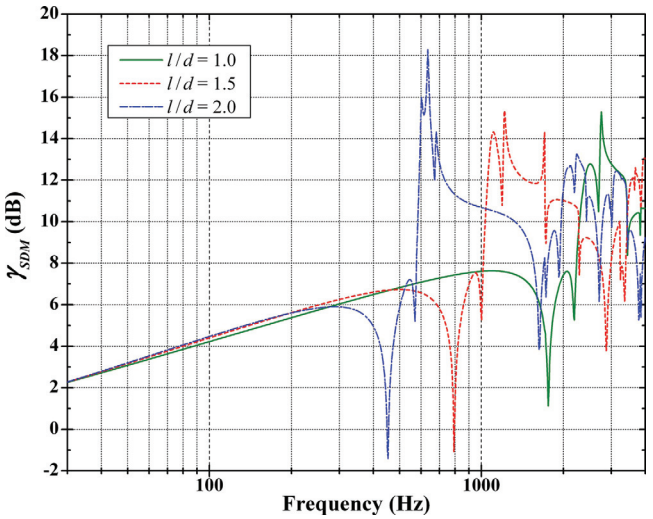

FIG. 7. (Color online) Tendency plot of γ_{SDM} versus frequency for orthogonally rib-stiffened double-panel structures filled by air with selected structural geometry ratios: normal sound incident case.

which can be normalized as

$$\bar{D}_x = D_x/Ed^3, \ \bar{D}_y = D_y/Ed^3. \quad (50)$$

For $t_x = t_y$ and $l_x = l_y$ as in the present study, $\bar{D}_x = \bar{D}_y$ and hence one can use only one symbol $\bar{D}$ to represent both $\bar{D}_x$ and $\bar{D}_y$. It should be pointed out that the fiberglass is loosely filled into the partitioned cavity and not bonded to the panels/rib-stiffeners, and hence has no contribution to the structural rigidity $\bar{D}$.

Incorporating the above defined dimensionless parameters $\bar{M}$, $\bar{D}$, and the sound insulation index STL, one may define an integrated index for optimal design toward high-stiffness-to-mass ratio and superior sound isolation capability as

$$\gamma_{SDM} = \frac{STL \times \bar{D}}{\bar{M}}. \quad (51)$$

The larger the integrated index γ_{SDM} is the more superior the combined acoustic and structural performance of the double-panel will be.

Figures 7 and 8 show the tendency plots of γ_{SDM} versus frequency for orthogonally rib-stiffened double-panel structures having cavities filled separately with air and fiberglass. The influence of the key geometry ratio l/d on the integrated index γ_{SDM} is explored by comparing three typical cases, i.e., $l/d = 1.0$, 1.5, and 2.0. It is observed from Figs. 7 and 8 that whilst l/d has negligible influence on γ_{SDM} at low frequencies (<300 Hz), it causes significant changes of γ_{SDM} at relatively high frequencies. This implies that the integrated performance of the double-panel including mass, stiffness, and STL can be designed and optimized by varying the key structural geometry ratio ld. Generally speaking, a larger l/d will help the structure to achieve a higher integrated index γ_{SDM}.

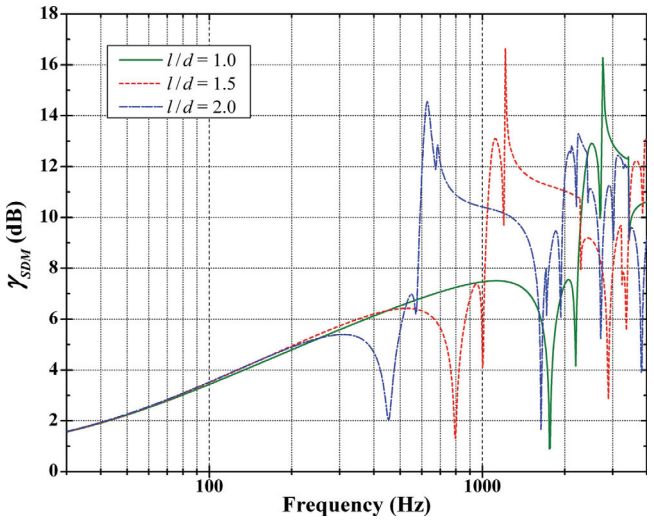

FIG. 8. (Color online) Tendency plot of γ_{SDM} versus frequency for orthogonally rib-stiffened double-panel structures filled with fiberglass for selected structural geometry ratios: normal sound incident case.

Relative to Fig. 7, the corresponding curves in Fig. 8 have slight alterations, resulting from the inclusion of fiberglass that induces changes in the parameters $\bar{M}$ and STL. In terms of the present optimal algorithm of Eq. (51), the inclusion of fiberglass does not appear to present additional benefits for the integrated performance. However, in accordance with different engineering requirements, the weight of the three parameters STL, $\bar{D}$, and $\bar{M}$ can be alternatively selected and thus different optimal designs may be achieved.

IV. CONCLUSIONS

Focusing on lightweight composite double-panel structures commonly used as aircraft fuselages, we propose a theoretical model to tackle with the sound transmission problem of infinite orthogonally rib-stiffened double-panel structures with fiberglass filled within the partitioned cavities. The process of sound penetration across the fiberglass is characterized by adopting the equivalent fluid model. The effects of fluid-structure coupling are also fully included by enforcing velocity continuity conditions at fluid-panel interfaces. The space-harmonic approach and the virtual work principle are applied to solve the resultant governing equations of the whole system. For validity check, the model predictions are compared with existing theoretical and experimental results for a simplified version of the double-panel structure, with good agreements achieved.

The model is subsequently applied to examine the influence of the cavity-filling fiberglass on sound transmission across the whole structure. It is demonstrated that the fluid-structure coupling effects should be taken into account in any theoretical attempt, especially when they play a role comparable with that of the rib-stiffeners when the rib-stiffener separations are sufficiently large. The inclusion of the fiberglass leads to remarkable changes of the STL versus frequency curves at low frequencies.

As a highlight of this research, an integrated optimal algorithm toward lightweight, high-stiffness, and superior sound insulation capability is proposed. With one key structural geometry ratio selected as the variable, a preliminary optimal design of the double-panel structure is carried out. It is found that the structural geometry ratio plays a significant role in the integrated mechanical and acoustical performance of the structure, providing, therefore, fundamental insight into the multifunctional design of the structure.

ACKNOWLEDGMENTS

The theoretical and experimental results from J. Legault and N. Atalla are employed to construct Fig. 3, which is appreciated. This work is supported by the National Basic Research Program of China (2011CB6103005), the National 111 Project of China (B06024), and the National Natural Science Foundation of China (11072188 and 10825210) the Shaanxi Province 13115 project (S2010ZDKG704).

APPENDIX A: TENSIONAL FORCES, BENDING MOMENTS AND TORSIONAL MOMENTS OF RIB-STIFFENERS

Adopting the similar procedure of Takahashi's beam model[33] for rib-stiffeners, taking the inertial effects of the rib-stiffeners into consideration and applying the Hooke's law and the Newton's second law, one can obtain the tensional forces of the rib-stiffeners as[13]

$$Q_x^+ = -\frac{K_x(K_x - m_x\omega^2)}{2k_x - m_x\omega^2}w_1 + \frac{K_x^2}{2K_x - m_x\omega^2}w_2 \tag{A1}$$

$$Q_x^- = -\frac{K_x^2}{2K_x - m_x\omega^2}w_1 + \frac{K_x(K_x - m_x\omega^2)}{2K_x - m_x\omega^2}w_2, \tag{A2}$$

$$Q_y^+ = -\frac{K_y(K_y - m_y\omega^2)}{2K_y - m_y\omega^2}w_1 + \frac{K_y^2}{2K_y - m_y\omega^2}w_2, \tag{A3}$$

$$Q_y^- = -\frac{K_y^2}{2K_y - m_y\omega^2}w_1 + \frac{K_y(K_y - m_y\omega^2)}{2K_y - m_y\omega^2}w_2, \tag{A4}$$

where ω is the circular frequency, K_x and K_y are the tensional stiffness of half rib-stiffeners per unit length, and m_x and m_y are the line mass density of the x- and y-wise stiffeners, respectively.

Likewise, the bending moments of the rib-stiffeners can be expressed as[13]

$$M_x^+ = \frac{E_xI_x^*(E_xI_x^* - \rho_xI_x\omega^2)}{2E_xI_x^* - \rho_xI_x\omega^2}\frac{\partial^2 w_1}{\partial x^2} - \frac{E_x^2I_x^{*2}}{2E_xI_x^* - \rho_xI_x\omega^2}\frac{\partial^2 w_2}{\partial x^2}, \tag{A5}$$

$$M_x^- = \frac{E_x^2I_x^{*2}}{2E_xI_x^* - \rho_xI_x\omega^2}\frac{\partial^2 w_1}{\partial x^2} - \frac{E_xI_x^*(E_xI_x^* - \rho_xI_x\omega^2)}{2E_xI_x^* - \rho_xI_x\omega^2}\frac{\partial^2 w_2}{\partial x^2}, \tag{A6}$$

$$M_x^+ = \frac{E_y I_y^* \left(E_y I_y^* - \rho_y I_y \omega^2\right)}{2E_y I_y^* - \rho_y I_y \omega^2} \frac{\partial^2 w_1}{\partial y^2} - \frac{E_y^2 I_y^{*2}}{2E_y I_y^* - \rho_y I_y \omega^2} \frac{\partial^2 w_2}{\partial y^2}, \tag{A7}$$

$$M_y^- = \frac{E_y^2 I_y^{*2}}{2E_y I_y^* - \rho_y I_y \omega^2} \frac{\partial^2 w_1}{\partial y^2} - \frac{E_y I_y^* \left(E_y I_y^* - \rho_y I_y \omega^2\right)}{2E_y I_y^* - \rho_y I_y \omega^2} \frac{\partial^2 w_2}{\partial y^2}, \tag{A8}$$

where $(E_x I_x^*, E_y I_y^*)$ are the bending stiffness of half rib-stiffeners per unit length and (ρ_x, ρ_y), (I_x, I_y) are the mass density and polar moment of inertia of the stiffeners, respectively, with subscripts x and y indicating the corresponding orientations of the stiffeners.

In a similar scheme, the torsional moments of the rib-stiffeners are given by[13]

$$M_{Tx}^+ = \frac{G_x J_x^* \left(G_x J_x^* - \rho_x J_x \omega^2\right)}{2G_x J_x^* - \rho_x J_x \omega^2} \frac{\partial^2 w_1}{\partial x \partial y} - \frac{G_x^2 J_x^{*2}}{2G_x J_x^* - \rho_x J_x \omega^2} \frac{\partial^2 w_2}{\partial x \partial y} \tag{A9}$$

$$M_{Tx}^- = \frac{G_x^2 J_x^{*2}}{2G_x J_x^* - \rho_x J_x \omega^2} \frac{\partial^2 w_1}{\partial x \partial y} - \frac{G_x J_x^* \left(G_x J_x^* - \rho_x J_x \omega^2\right)}{2G_x J_x^* - \rho_x J_x \omega^2} \frac{\partial^2 w_2}{\partial x \partial y}, \tag{A10}$$

$$M_{Ty}^+ = \frac{G_y J_y^* \left(G_y J_y^* - \rho_y J_y \omega^2\right)}{2G_y J_y^* - \rho_y J_y \omega^2} \frac{\partial^2 w_1}{\partial y \partial x} - \frac{G_y^2 J_y^{*2}}{2G_y J_y^* - \rho_y J_y \omega^2} \frac{\partial^2 w_2}{\partial y \partial x}, \tag{A11}$$

$$M_{Ty}^- = \frac{G_y^2 J_y^{*2}}{2G_y J_y^* - \rho_y J_y \omega^2} \frac{\partial^2 w_1}{\partial y \partial x} - \frac{G_y J_y^* \left(G_y J_y^* - \rho_y J_y \omega^2\right)}{2G_y J_y^* - \rho_y J_y \omega^2} \frac{\partial^2 w_2}{\partial y \partial x}, \tag{A12}$$

where $(G_x J_x^*, G_y J_y^*)$ are the torsional stiffness of half rib-stiffeners per unit length and (J_x, J_y) are the torsional moments of inertia of the stiffeners.

To simplify Eqs. (A1)–(A12), the following sets of specified characteristics are utilized to replace the coefficients of the general displacements.

(1) Replacement of tensional force coefficients

$$R_{Q1} = \frac{K_x (K_x - m_x \omega^2)}{2K_x - m_x \omega^2}, \quad R_{Q2} = \frac{K_x^2}{2K_x - m_x \omega^2}, \tag{A13}$$

$$R_{Q3} = \frac{K_y \left(K_y - m_y \omega^2\right)}{2K_y - m_y \omega^2}, \quad R_{Q4} = \frac{K_y^2}{2K_y - m_y \omega^2}. \tag{A14}$$

(2) Replacement of bending moment coefficients

$$R_{M1} = \frac{E_x I_x^* \left(E_x I_x^* - \rho_x I_x \omega^2\right)}{2E_x I_x^* - \rho_x I_x \omega^2}, \quad R_{M2} = \frac{E_x^2 I_x^{*2}}{2E_x I_x^* - \rho_x I_x \omega^2}, \tag{A15}$$

$$R_{M3} = \frac{E_y I_y^* \left(E_y I_y^* - \rho_y I_y \omega^2\right)}{2E_y I_y^* - \rho_y I_y \omega^2}, \quad R_{M4} = \frac{E_y^2 I_y^{*2}}{2E_y I_y^* - \rho_y I_y \omega^2}. \tag{A16}$$

(3) Replacement of torsional moment coefficients

$$R_{T1} = \frac{G_x J_x^* \left(G_x J_x^* - \rho_x J_x \omega^2\right)}{2G_x J_x^* - \rho_x J_x \omega^2}, \quad R_{T2} = \frac{G_x^2 J_x^{*2}}{2G_x J_x^* - \rho_x J_x \omega^2}, \tag{A17}$$

$$R_{T3} = \frac{G_y J_y^* \left(G_y J_y^* - \rho_y J_y \omega^2\right)}{2G_y J_y^* - \rho_y J_y \omega^2}, \quad R_{T4} = \frac{G_y^2 J_y^{*2}}{2G_y J_y^* - \rho_y J_y \omega^2}. \tag{A18}$$

In terms of space-harmonic series, the expressions of the tensional forces, bending moments, and torsional moments can be simplified as follows:

(1) Tensional forces

$$Q_x^+ = \sum_{m=-\infty}^{+\infty} \sum_{n=-\infty}^{+\infty} \left(-R_{Q1} \alpha_{1,mn} + R_{Q2} \alpha_{2,mn}\right) e^{-i(\alpha_m x + \beta_n y)}, \tag{A19}$$

$$Q_x^- = \sum_{m=-\infty}^{+\infty} \sum_{n=-\infty}^{+\infty} \left(-R_{Q2} \alpha_{1,mn} + R_{Q1} \alpha_{2,mn}\right) e^{-i(\alpha_m x + \beta_n y)}, \tag{A20}$$

$$Q_y^+ = \sum_{m=-\infty}^{+\infty} \sum_{n=-\infty}^{+\infty} \left(-R_{Q3} \alpha_{1,mn} + R_{Q4} \alpha_{2,mn}\right) e^{-i(\alpha_m x + \beta_n y)}, \tag{A21}$$

$$Q_y^- = \sum_{m=-\infty}^{+\infty} \sum_{n=-\infty}^{+\infty} \left(-R_{Q4} \alpha_{1,mn} + R_{Q3} \alpha_{2,mn}\right) e^{-i(\alpha_m x + \beta_n y)}. \tag{A22}$$

(2) Bending moments

$$M_x^+ = \sum_{m=-\infty}^{+\infty} \sum_{n=-\infty}^{+\infty} \left(-R_{M1} \alpha_{1,mn} + R_{M2} \alpha_{2,mn}\right) \alpha_m^2 e^{-i(\alpha_m x + \beta_n y)}, \tag{A23}$$

$$M_x^- = \sum_{m=-\infty}^{+\infty} \sum_{n=-\infty}^{+\infty} \left(-R_{M2} \alpha_{1,mn} + R_{M1} \alpha_{2,mn}\right) \alpha_m^2 e^{-i(\alpha_m x + \beta_n y)}, \tag{A24}$$

$$M_y^+ = \sum_{m=-\infty}^{+\infty} \sum_{n=-\infty}^{+\infty} \left(-R_{M3} \alpha_{1,mn} + R_{M4} \alpha_{2,mn}\right) \beta_n^2 e^{-i(\alpha_m x + \beta_n y)}, \tag{A25}$$

$$M_y^- = \sum_{m=-\infty}^{+\infty} \sum_{n=-\infty}^{+\infty} \left(-R_{M4} \alpha_{1,mn} + R_{M3} \alpha_{2,mn}\right) \beta_n^2 e^{-i(\alpha_m x + \beta_n y)}. \tag{A26}$$

(3) Torsional moments

$$M_{Tx}^{+}=\sum_{m=-\infty}^{+\infty}\sum_{n=-\infty}^{+\infty}\left(-R_{T1}\alpha_{1,mn}+R_{T2}\alpha_{2,mn}\right)\alpha_m\beta_n e^{-i(\alpha_m x+\beta_n y)}, \tag{A27}$$

$$M_{Tx}^{-}=\sum_{m=-\infty}^{+\infty}\sum_{n=-\infty}^{+\infty}\left(-R_{T2}\alpha_{1,mn}+R_{T1}\alpha_{2,mn}\right)\alpha_m\beta_n e^{-i(\alpha_m x+\beta_n y)}, \tag{A28}$$

$$M_{Ty}^{+}=\sum_{m=-\infty}^{+\infty}\sum_{n=-\infty}^{+\infty}\left(-R_{T3}\alpha_{1,mn}+R_{T4}\alpha_{2,mn}\right)\alpha_m\beta_n e^{-i(\alpha_m x+\beta_n y)}, \tag{A29}$$

$$M_{Ty}^{-}=\sum_{m=-\infty}^{+\infty}\sum_{n=-\infty}^{+\infty}\left(-R_{T4}\alpha_{1,mn}+R_{T3}\alpha_{2,mn}\right)\alpha_m\beta_n e^{-i(\alpha_m x+\beta_n y)}. \tag{A30}$$

APPENDIX B: EERIVATION OF EQUATION (44)

The deflection coefficients of the two face panels are

$$\{\alpha_{1,kl}\}=[\alpha_{1,11}\quad\alpha_{1,21}\quad\cdots\quad\alpha_{1,K1}\quad\alpha_{1,12}\quad\alpha_{1,22}\quad\cdots\quad\alpha_{1,K2}\quad\cdots\quad\alpha_{1,KL}]^{\mathrm{T}}_{KL\times 1}, \tag{B1}$$

$$\{\alpha_{2,kl}\}=[\alpha_{2,11}\quad\alpha_{2,21}\quad\cdots\quad\alpha_{2,K1}\quad\alpha_{2,12}\quad\alpha_{2,22}\quad\cdots\quad\alpha_{2,K2}\quad\cdots\quad\alpha_{2,KL}]^{\mathrm{T}}_{KL\times 1}. \tag{B2}$$

The left-hand side of Eq. (44) represents the generalized force, that is,

$$\{F_{kl}\}=[F_{11}\quad F_{21}\quad\cdots\quad F_{K1}\quad F_{12}\quad F_{F22}\quad\cdots\quad F_{K2}\quad\cdots\quad F_{KL}]^{\mathrm{T}}_{KL\times 1}, \tag{B3}$$

$$F_{kl}=\begin{cases}2Il_x l_y & \text{at } k=\frac{K+1}{2} \text{ and } l=\frac{L+1}{2}\\ 0 & \text{at } k\neq\frac{K+1}{2}\,||\,l\neq\frac{L+1}{2}\end{cases} \tag{B4}$$

$$\lambda_{kl}^{11,1}=\left[D_1(\alpha_k^2+\beta_l^2)^2-m_1\omega^2-\frac{w^2\rho_0}{ik_{z,kl}}+\frac{\omega^2\rho_{\mathrm{cav}}(k_{z,cav,kl}d)}{k_{z,cav,kl}\sin(k_{z,cav,kl}d)}\right].\,l_x l_y, \tag{B5}$$

$$T_{11,1}=\mathrm{diag}[\lambda_{11}^{11,1}\quad\lambda_{21}^{11,1}\quad\cdots\quad\lambda_{K1}^{11,1}\quad\lambda_{12}^{11,1}\quad\lambda_{22}^{11,1}\quad\cdots\quad\lambda_{K2}^{11,1}\quad\cdots\quad\lambda_{KL}^{11,1}]_{KL\times KL}, \tag{B6}$$

$$\lambda_{KL}^{11,2}=l_x\times\mathrm{diag}[R_{Q1}-l\alpha_1^3R_{M1}\quad R_{Q1}-i\alpha_2^3R_{M1}\quad\cdots\quad R_{Q1}-i\alpha_K^3R_{M1}]_{K\times L}, \tag{B7}$$

$$T_{11,2}=\begin{bmatrix}\lambda_{KL}^{11,2} & \lambda_{KL}^{11,2} & \cdots & \lambda_{KL}^{11,2}\\ \lambda_{KL}^{11,2} & \lambda_{KL}^{11,2} & \cdots & \lambda_{KL}^{11,2}\\ \vdots & \vdots & \ddots & \vdots\\ \lambda_{KL}^{11,2} & \lambda_{KL}^{11,2} & \cdots & \lambda_{KL}^{11,2}\end{bmatrix}_{Kl\times KL}, \tag{B8}$$

$$\lambda_{Kl,n}^{11,3}=l_x\times\mathrm{diag}[-i\alpha_1\beta_l\beta_n R_{T1}\quad -i\alpha_2\beta_l\beta_n R_{T1}\quad\cdots\quad i\alpha_K\beta_l\beta_n R_{T1}]_{K\times L}, \tag{B9}$$

$$T_{11,3}=\begin{bmatrix}\lambda_{K1,1}^{11,3} & \lambda_{K1,2}^{11,3} & \cdots & \lambda_{K1,L}^{11,3}\\ \lambda_{K2,1}^{11,3} & \lambda_{K2,2}^{11,3} & \cdots & \lambda_{K2,L}^{11,3}\\ \vdots & \vdots & \ddots & \vdots\\ \lambda_{KL,1}^{11,3} & \lambda_{KL,2}^{11,3} & \cdots & \lambda_{KL,L}^{11,3}\end{bmatrix}_{Kl\times KL}, \tag{B10}$$

$$\lambda_{K}^{11,4}=l_y\times\begin{bmatrix}R_{Q3}-i\beta_l^3R_{M3} & R_{Q3}-i\beta_l^3R_{M3} & \cdots & R_{Q3}-i\beta_l^3R_{M3}\\ R_{Q3}-i\beta_l^3R_{M3} & R_{Q3}-i\beta_l^3R_{M3} & \cdots & R_{Q3}-i\beta_l^3R_{M3}\\ \vdots & \vdots & \ddots & \vdots\\ R_{Q3}-i\beta_l^3R_{M3} & R_{Q3}-i\beta_l^3R_{M3} & \cdots & R_{Q3}-i\beta_l^3R_{M3}\end{bmatrix}_{K\times L}, \tag{B11}$$

$$T_{11,4}=\mathrm{diag}[\lambda_{\mathrm{K1}}^{11,4}\quad\lambda_{K2}^{11,4}\quad\cdots\quad\lambda_{KL}^{11,4}]_{KL\times KL}, \tag{B12}$$

$$\lambda_{KL}^{11,5} = l_y \times \begin{bmatrix} -i\alpha_1\beta_l\alpha_1 R_{T3} & -i\alpha_1\beta_l\alpha_2 R_{T3} & \cdots & -i\alpha_1\beta_l\alpha_K R_{T3} \\ -i\alpha_2\beta_l\alpha_1 R_{T3} & -i\alpha_2\beta_l\alpha_2 R_{T3} & \cdots & -i\alpha_2\beta_l\alpha_K R_{T3} \\ \vdots & \vdots & \ddots & \vdots \\ -i\alpha_K\beta_l\alpha_1 R_{T3} & -i\alpha_K\beta_l\alpha_2 R_{T3} & \cdots & -i\alpha_K\beta_l\alpha_K R_{T3} \end{bmatrix}_{K\times L}, \tag{B13}$$

$$T_{11,5} = \mathrm{diag}[\,\lambda_{K1}^{11,5} \quad \lambda_{K2}^{11,5} \quad \cdots \quad \lambda_{KL}^{11,5}]_{KL\times Kl}, \tag{B14}$$

$$\lambda_{kl}^{12,1} = -\frac{\omega^2\rho_{\mathrm{cav}}}{k_{z,\mathrm{cav},kl}\sin(K_{z,\mathrm{cav}.kl}d)}\cdot l_x l_y, \tag{B15}$$

$$T_{12,1} = \mathrm{diag}[\,\lambda_{11}^{12,1} \quad \lambda_{21}^{12,1} \quad \cdots \quad \lambda_{K1}^{12,1} \quad \lambda_{12}^{12,1} \quad \lambda_{22}^{12,1} \quad \cdots \quad \lambda_{K2}^{12,1} \quad \cdots \quad \lambda_{KL}^{12,1}]_{KL\times KL}, \tag{B16}$$

$$\lambda_{KL}^{12,2} = l_x \times \mathrm{diag}[\,-R_{Q2} + i\alpha_1^3 R_{M2} \quad -R_{Q2} + i\alpha_2^3 R_{M2} \quad \cdots \quad -R_{Q2} + i\alpha_K^3 R_{M2}]_{K\times L}, \tag{B17}$$

$$T_{12,2} = \begin{bmatrix} \lambda_{KL}^{12,2} & \lambda_{KL}^{12,2} & \cdots & \lambda_{KL}^{12,2} \\ \lambda_{KL}^{12,2} & \lambda_{KL}^{12,2} & \cdots & \lambda_{KL}^{12,2} \\ \vdots & \vdots & \ddots & \vdots \\ \lambda_{KL}^{12,2} & \lambda_{KL}^{12,2} & \cdots & \lambda_{KL}^{12,2} \end{bmatrix}_{KL\times KL}, \tag{B18}$$

$$\lambda_{Kl,n}^{12,3} = l_x \times \mathrm{diag}[\,i\alpha_1\beta_l\beta_n R_{T2} \quad i\alpha_2\beta_l\beta_n R_{T2} \quad \cdots \quad i\alpha_K\beta_l\beta_n R_{T2}]_{K\times L}, \tag{B19}$$

$$T_{12,3} = \begin{bmatrix} \lambda_{K1,1}^{12,3} & \lambda_{K1,2}^{12,3} & \cdots & \lambda_{K1,L}^{12,3} \\ \lambda_{K2,1}^{12,3} & \lambda_{K2,2}^{12,3} & \cdots & \lambda_{K2,L}^{12,3} \\ \vdots & \vdots & \ddots & \vdots \\ \lambda_{KL,1}^{12,3} & \lambda_{KL,2}^{12,3} & \cdots & \lambda_{KL,L}^{12,3} \end{bmatrix}_{KL\times KL}, \tag{B20}$$

$$\lambda_{Kl}^{12,4} = l_y \times \begin{bmatrix} -R_{Q4} + i\beta_l^3 R_{M4} & -R_{Q4} + i\beta_l^3 R_{M4} & \cdots & -R_{Q4} + i\beta_l^3 R_{M4} \\ -R_{Q4} + i\beta_l^3 R_{M4} & -R_{Q4} + i\beta_l^3 R_{M4} & \cdots & -R_{Q4} + i\beta_l^3 R_{M4} \\ \vdots & \vdots & \ddots & \vdots \\ -R_{Q4} + i\beta_l^3 R_{M4} & -R_{Q4} + i\beta_l^3 R_{M4} & \cdots & -R_{Q4} + i\beta_l^3 R_{M4} \end{bmatrix}_{K\times L}, \tag{B21}$$

$$T_{12,4} = \mathrm{diag}[\,\lambda_{K1}^{12,4} \quad \lambda_{K2}^{12,4} \quad \cdots \quad \lambda_{KL}^{12,4}]_{KL\times KL}, \tag{B22}$$

$$\lambda_{K1}^{12,5} = l_y \times \begin{bmatrix} i\alpha_1\beta_l\alpha_1 R_{T4} & i\alpha_1\beta_l\alpha_2 R_{T4} & \cdots & i\alpha_1\beta_l\alpha_K R_{T4} \\ i\alpha_2\beta_l\alpha_1 R_{T4} & i\alpha_2\beta_l\alpha_2 R_{T4} & \cdots & i\alpha_2\beta_l\alpha_K R_{T4} \\ \vdots & \vdots & \ddots & \vdots \\ i\alpha_K\beta_l\alpha_1 R_{T4} & i\alpha_K\beta_l\alpha_2 R_{T4} & \cdots & i\alpha_K\beta_l\alpha_K R_{T4} \end{bmatrix}_{K\times L}, \tag{B23}$$

$$T_{12,5} = \mathrm{diag}[\,\lambda_{K1}^{12,5} \quad \lambda_{K2}^{12,5} \quad \cdots \quad \lambda_{KL}^{12,5}]_{KL\times KL}, \tag{B24}$$

$$\lambda_{kl}^{21,1} = -\frac{\omega^2\rho_{\mathrm{cav}}}{k_{z,\mathrm{cav},kl}\sin(k_{z,\mathrm{cav},kl}d)}\cdot l_x l_y, \tag{B25}$$

$$T_{21,1} = \mathrm{diag}[\,\lambda_{11}^{21,1} \quad \lambda_{21}^{21,1} \quad \cdots \quad \lambda_{K1}^{21,1} \quad \lambda_{12}^{21,1} \quad \lambda_{22}^{21,1} \quad \cdots \quad \lambda_{K2}^{21,1} \quad \cdots \quad \lambda_{KL}^{21,1}]_{KL\times KL}, \tag{B26}$$

$$\lambda_{KL}^{21,2} = l_x \times \mathrm{diag}[\,-R_{Q2} + i\alpha_1^3 R_{M2}\ \ -R_{Q2} + i\alpha_2^3 R_{M2}\ \ \cdots\ \ -R_{Q2} + i\alpha_K^3 R_{M2}]_{K\times L}\,, \tag{B27}$$

$$T_{21,2} = \begin{bmatrix} \lambda_{KL}^{21,2} & \lambda_{KL}^{21,2} & \cdots & \lambda_{KL}^{21,2} \\ \lambda_{KL}^{21,2} & \lambda_{KL}^{21,2} & \cdots & \lambda_{KL}^{21,2} \\ \vdots & \vdots & \ddots & \vdots \\ \lambda_{KL}^{21,2} & \lambda_{KL}^{21,2} & \cdots & \lambda_{KL}^{21,2} \end{bmatrix}_{KL\times KL}, \tag{B28}$$

$$\lambda_{Kl,n}^{21,3} = l_x \times \mathrm{diag}[\,i\alpha_1\beta_l\beta_n R_{T2}\quad i\alpha_2\beta_l\beta_n R_{T2}\quad \cdots\quad i\alpha_K\beta_l\beta_n R_{T2}]_{K\times L}\,, \tag{B29}$$

$$T_{21,3} = \begin{bmatrix} \lambda_{K1,1}^{21,3} & \lambda_{K1,2}^{21,3} & \cdots & \lambda_{K1,L}^{21,3} \\ \lambda_{K2,1}^{21,3} & \lambda_{K2,2}^{21,3} & \cdots & \lambda_{K2,L}^{21,3} \\ \vdots & \vdots & \ddots & \vdots \\ \lambda_{KL,1}^{21,3} & \lambda_{KL,2}^{21,3} & \cdots & \lambda_{KL,L}^{21,3} \end{bmatrix}_{KL\times KL}, \tag{B30}$$

$$\lambda_{Kl}^{21,4} = l_y \times \begin{bmatrix} -R_{Q4} + i\beta_l^3 R_{M4} & -R_{Q4} + i\beta_l^3 R_{M4} & \cdots & -R_{Q4} + i\beta_l^3 R_{M4} \\ -R_{Q4} + i\beta_l^3 R_{M4} & -R_{Q4} + i\beta_l^3 R_{M4} & \cdots & -R_{Q4} + i\beta_l^3 R_{M4} \\ \vdots & \vdots & \ddots & \vdots \\ -R_{Q4} + i\beta_l^3 R_{M4} & -R_{Q4} + i\beta_l^3 R_{M4} & \cdots & -R_{Q4} + i\beta_l^3 R_{M4} \end{bmatrix}_{K\times L}, \tag{B31}$$

$$T_{21,4} = \mathrm{diag}[\,\lambda_{K1}^{21,4}\quad \lambda_{K2}^{21,4}\quad \cdots\quad \lambda_{KL}^{21,4}]_{KL\times KL}\,, \tag{B32}$$

$$\lambda_{kl}^{21,5} = l_y \times \begin{bmatrix} i\alpha_1\beta_l\alpha_1 R_{T4} & i\alpha_1\beta_l\alpha_2 R_{T4} & \cdots & i\alpha_1\beta_l\alpha_K R_{T4} \\ i\alpha_2\beta_l\alpha_1 R_{T4} & i\alpha_2\beta_l\alpha_2 R_{T4} & \cdots & i\alpha_2\beta_l\alpha_K R_{T4} \\ \cdots & \cdots & \ddots & \vdots \\ i\alpha_K\beta_l\alpha_1 R_{T4} & i\alpha_K\beta_l\alpha_2 R_{T4} & \cdots & i\alpha_K\beta_l\alpha_K R_{T4} \end{bmatrix}_{K\times L}, \tag{B33}$$

$$T_{21,5} = \mathrm{diag}[\,\lambda_{K1}^{21,5}\quad \lambda_{K2}^{21,5}\quad \cdots\quad \lambda_{KL}^{21,5}]_{KL\times KL}\,, \tag{B34}$$

$$\lambda_{kl}^{22,1} = \left[D_2(\alpha_k^2 + \beta_l^2)^2 - m_2\omega^2 - \frac{\omega^2\rho_0}{ik_{z,kl}} + \frac{\omega^2\rho_{\mathrm{cav}}\cos(k_{z,\mathrm{cav},kl}d)}{k_{z,\mathrm{cav},kl}\sin(k_{z,\mathrm{cav},kl}d)}\right]\cdot l_x l_y, \tag{B35}$$

$$T_{22,1} = \mathrm{diag}[\,\lambda_{11}^{22,1}\quad \lambda_{21}^{22,1}\quad \cdots\quad \lambda_{K1}^{22,1}\quad \lambda_{12}^{22,1}\quad \lambda_{22}^{22,1}\quad \cdots\quad \lambda_{K2}^{22,1}\quad \cdots\quad \lambda_{KL}^{22,1}]_{KL\times KL}\,, \tag{B36}$$

$$\lambda_{KL}^{22,2} = l_x \times \mathrm{diag}[\,R_{Q1} - i\alpha_1^3 R_{M1}\quad R_{Q1} - i\alpha_2^3 R_{M1}\quad \cdots\quad R_{Q1} - i\alpha_K^3 R_{M1}]_{K\times L}\,, \tag{B37}$$

$$T_{22,2} = \begin{bmatrix} \lambda_{KL}^{22,2} & \lambda_{KL}^{22,2} & \cdots & \lambda_{KL}^{22,2} \\ \lambda_{KL}^{22,2} & \lambda_{KL}^{22,2} & \cdots & \lambda_{KL}^{22,2} \\ \vdots & \vdots & \ddots & \vdots \\ \lambda_{KL}^{22,2} & \lambda_{KL}^{22,2} & \cdots & \lambda_{KL}^{22,2} \end{bmatrix}_{KL\times KL}, \tag{B38}$$

$$\lambda_{Kl,n}^{22,3} = l_x \times \mathrm{diag}[\,-i\alpha_1\beta_l\beta_n\beta_{T1}\ \ -i\alpha_2\beta_l\beta_n\beta_{T1}\quad \cdots\quad -i\alpha_K\beta_l\beta_n\beta_{T1}]_{K\times L}\,, \tag{B39}$$

$$T_{22,3} = \begin{bmatrix} \lambda_{K1,1}^{22,3} & \lambda_{K1,2}^{22,3} & \cdots & \lambda_{K1,L}^{22,3} \\ \lambda_{K2,1}^{22,3} & \lambda_{K2,2}^{22,3} & \cdots & \lambda_{K2,L}^{22,3} \\ \vdots & \vdots & \ddots & \vdots \\ \lambda_{KL,1}^{22,3} & \lambda_{KL,2}^{22,3} & \cdots & \lambda_{KL,L}^{22,3} \end{bmatrix}_{KL\times KL}, \tag{B40}$$

$$\lambda_{Kl}^{22,4} = l_y \times \begin{bmatrix} R_{Q3} - i\beta_l^3 R_{M3} & R_{Q3} - i\beta_l^3 R_{M3} & \cdots & R_{Q3} - i\beta_l^3 R_{M3} \\ R_{Q3} - i\beta_l^3 R_{M3} & R_{Q3} - i\beta_l^3 R_{M3} & \cdots & R_{Q3} - i\beta_l^3 R_{M3} \\ \vdots & \vdots & \ddots & \vdots \\ R_{Q3} - i\beta_l^3 R_{M3} & R_{Q3} - i\beta_l^3 R_{M3} & \vdots & R_{Q3} - i\beta_l^3 R_{M3} \end{bmatrix}_{K\times L}, \tag{B41}$$

$$T_{22,4} = \mathrm{diag}[\ \lambda_{K1}^{22,4} \quad \lambda_{K2}^{22,4} \quad \cdots \quad \lambda_{KL}^{22,4}\ ]_{KL\times KL}, \tag{B42}$$

$$\lambda_{Kl}^{22,5} = l_y \times \begin{bmatrix} -i\alpha_1\beta_l\alpha_1 R_{T3} & -i\alpha_1\beta_l\alpha_2 R_{T3} & \cdots & -i\alpha_1\beta_l\alpha_K R_{T3} \\ -i\alpha_2\beta_l\alpha_1 R_{T3} & -i\alpha_2\beta_l\alpha_2 R_{T3} & \cdots & -i\alpha_2\beta_l\alpha_K R_{T3} \\ \vdots & \vdots & \ddots & \vdots \\ -i\alpha_K\beta_l\alpha_1 R_{T3} & -i\alpha_K\beta_l\alpha_2 R_{T3} & \cdots & -i\alpha_K\beta_l\alpha_K R_{T3} \end{bmatrix}_{K\times L}. \tag{B43}$$

$$T_{22,5} = \mathrm{diag}[\ \lambda_{K1}^{22,5} \quad \lambda_{K2}^{22,5} \quad \cdots \quad \lambda_{KL}^{22,5}\ ]_{KL\times KL}. \tag{B44}$$

Using the definition of the sup-matrices presented above, one obtains

$$\begin{aligned} T_{11} &= T_{11,1} + T_{11,2} + T_{11,3} + T_{11,4} + T_{11,5}, \\ T_{22} &= T_{22,1} + T_{22,2} + T_{22,3} + T_{22,4} + T_{22,5}, \end{aligned} \tag{B45}$$

$$\begin{aligned} T_{12} &= T_{12,1} + T_{12,2} + T_{12,3} + T_{12,4} + T_{12,5}, \\ T_{22} &= T_{22,1} + T_{22,2} + T_{22,3} + T_{22,4} + T_{22,5}. \end{aligned} \tag{B46}$$

[1] B. R. Mace, "Periodically stiffened fluid-loaded plates, I: Response to convected harmonic pressure and free wave propagation," J. Sound Vib. **73**, 473–486 (1980a).
[2] B. R. Mace, "Sound radiation from a plate reinforced by two sets of parallel stiffeners," J. Sound Vib. **71**, 435–441 (1980b).
[3] B. R. Mace, "Sound radiation from fluid loaded orthogonally stiffened plates," J. Sound Vib. **79**, 439–452 (1981).
[4] D. J. Mead and K. K. Pujara, "Space-harmonic analysis of periodically supported beams: Response to convected random loading," J. Sound Vib. **14**, 525–532 (1971).
[5] J. H. Lee and J. Kim, "Analysis of sound transmission through periodically stiffened panels by space-harmonic expansion method," J. Sound Vib. **251**, 349–366 (2002).
[6] F. X. Xin and T. J. Lu, "Analytical and experimental investigation on transmission loss of clamped double panels: Implication of boundary effects," J. Acoust. Soc. Am. **125**, 1506–1517 (2009).
[7] F. X. Xin, T. J. Lu, and C. Q. Chen, "Vibroacoustic behavior of clamp mounted double-panel partition with enclosure air cavity," J. Acoust. Soc. Am. **124**, 3604–3612 (2008).
[8] G.-F. Lin and J. M. Garrelick, "Sound transmission through periodically framed parallel plates," J. Acoust. Soc. Am. **61**, 1014–1018 (1977).
[9] J. Wang, T. J. Lu, J. Woodhouse, R. S. Langley, and J. Evans, "Sound transmission through lightweight double-leaf partitions: Theoretical modelling," J. Sound Vib. **286**, 817–847 (2005).
[10] X. W. Yin, X. J. Gu, H. F. Cui, and R. Y. Shen, "Acoustic radiation from a laminated composite plate reinforced by doubly periodic parallel stiffeners," J. Sound Vib. **306**, 877–889 (2007).
[11] J. Legault and N. Atalla, "Numerical and experimental investigation of the effect of structural links on the sound transmission of a lightweight double panel structure," J. Sound Vib. **324**, 712–732 (2009).
[12] J. Legault and N. Atalla, "Sound transmission through a double panel structure periodically coupled with vibration insulators," J. Sound Vib. **329**, 3082–3100 (2010).
[13] F. X. Xin and T. J. Lu, "Analytical modeling of fluid loaded orthogonally rib-stiffened sandwich structures: Sound transmission," J. Mech. Phys. Solids **58**, 1374–1396 (2010).
[14] D. J. Mead, "Free wave propagation in periodically supported, infinite beams," J. Sound Vib. **11**, 181–197 (1970).
[15] F. X. Xin and T. J. Lu, "Sound radiation of orthogonally rib-stiffened sandwich structures with cavity absorption," Compos. Sci. Technol. **70**, 2198–2206 (2010).
[16] F. X. Xin and T. J. Lu, "Analytical modeling of sound transmission across finite aeroelastic panels in convected fluids," J. Acoust. Soc. Am. **128**, 1097–1107 (2010).
[17] T. J. Lu, A. Hess, and M. F. Ashby, "Sound absorption in metallic foams," J. Appl. Phys. **85**, 7528–7539 (1999).
[18] X. L. Wang and T. J. Lu, "Optimized acoustic properties of cellular solids," J. Acoust. Soc. Am. **106**, 756–765 (1999).
[19] T. J. Lu, F. Chen, and D. He, "Sound absorption of cellular metals with semiopen cells," J. Acoust. Soc. Am. **108**, 1697–1709 (2000).
[20] R. Panneton and N. Atalla, "Numerical prediction of sound transmission through finite multilayer systems with poroelastic materials," J. Acoust. Soc. Am. **100**, 346–354 (1996).
[21] M. E. Delany and E. N. Bazley, "Acoustical properties of fibrous absorbent materials," Appl. Acoust. **3**, 105–116 (1970).
[22] J.-F. Allard and Y. Champoux, "New empirical equations for sound propagation in rigid frame fibrous materials," J. Acoust. Soc. Am. **91**, 3346–3353 (1992).
[23] A. Trochidis and A. Kalaroutis, "Sound transmission through double partitions with cavity absorption," J. Sound Vib. **107**, 321–327 (1986).
[24] J. Alba, J. Ramis, and V. J. Sanchez-Morcillo, "Improvement of the prediction of transmission loss of double partitions with cavity absorption by minimization techniques," J. Sound Vib. **273**, 793–804 (2004).
[25] J. F. Allard. *Propagation of Sound in Porous Media*: *Modelling Sound Absorbing Materials* (Elsevier, London and New York, 1993).

[26]F. X. Xin, T. J. Lu, and C. Q. Chen, "External mean flow influence on noise transmission through double-leaf aeroelastic plates," AIAA J. **47**, 1939–1951 (2009).
[27]F. X. Xin, T. J. Lu, and C. Q. Chen, "Dynamic response and acoustic radiation of double-leaf metallic panel partition under sound excitation," Comput. Mater. Sci. **46**, 728–732 (2009).
[28]L. Brillouin, *Wave Propagation in Periodic Structures* (Dover, New York, 1953).
[29]F. X. Xin, T. J. Lu, and C. Q. Chen, "Sound transmission through simply supported finite double-panel partitions with enclosed air cavity," ASME J. Vibr. Acoust. **132**(011008), 1–11 (2010).
[30]W. R. Graham, "High-frequency vibration and acoustic radiation of fluid-loaded plates," Proc. R. Soc. London A. **352**, 1–43 (1995).
[31]H. Kolsters and P. Wennhage, "Optimisation of laser-welded sandwich panels with multiple design constraints," Mar. Struct. **22**, 154–171 (2009).
[32]T. S. Lok and Q. H. Cheng, "Elastic deflection of thin-walled sandwich panel," J. Sandw. Struct. Mater. **1**, 279–298 (1999).
[33]D. Takahashi, "Sound radiation from periodically connected double-plate structures," J. Sound Vib. **90**, 541–557 (1983).